Int. J. Heat Mass Transfer. Vol. 36, No. 11, pp. 2881–2890, 1993
Printed in Great Britain

0017–9310/93 $6.00 + 0.00

Natural convection and heat transfer in a vertical cavity filled with an ice–water saturated porous medium

XIAOLI ZHANG
Department of Mechanical Engineering, Ecole Polytechnique de Montréal, Montréal, Québec, Canada H3C 3A7

(*Received* 25 *June* 1992 *and in final form* 5 *October* 1992)

Abstract—A numerical study is made of natural convection and heat transfer in a rectangular porous cavity filled with an ice–water saturated porous medium. The two vertical sides of the cavity are cooled and heated at temperatures below and above the fusion point. The remaining sides of the cavity are assumed perfectly insulated. Special attention is focused on the influence of the heating temperature on the steady solutions. The Landau-transformation is used to immobilize the ice–water interface and the Darcy–Boussinesq equations are solved by the finite-difference technique. It is found that local maximum and minimum average Nusselt numbers occur at heating temperatures of 5 and 8°C, respectively. The melt region is wider at the bottom if the heating temperature is less than 8°C while the inverse is true for heating temperatures higher than 8°C. The 4°C isotherm is the boundary between the two counter-rotating flows at a heating temperature of 8°C only, otherwise the dominant flow crosses the 4°C isotherm and penetrates into the other layer as the heating temperature is higher than 4°C.

INTRODUCTION

RECENTLY, phase change heat transfer in enclosures, especially in a rectangular cavity, has attracted considerable interest due to its wide range of possible applications in the areas of thermal energy storage and high efficiency heat exchangers as well as in the food processing industry.

Studies on melting and solidification in a vertically heated cavity are usually based on the linear Boussinesq approximation where the buoyancy force is assumed to vary linearly with the temperature [1, 2]. It has been found that the solid–liquid interface is curved with the top section wider than the lower one and a higher melting rate in the upper part of the cavity, due to the convection flow with the fluid moving up along the heated wall and descending along the solid–liquid interface. It has also been well established that the average Nusselt number increases with an increasing heating temperature, if other parameters of the system are kept constant [1, 2].

However, the linear Boussinesq approximation commonly used in the above studies is not applicable for a number of fluids, such as water, molten bismuth, antimony, gallium and tellurium. For water, a maximum density occurs around 4°C at atmospheric pressure. It has been found [3, 4] that the average Nusselt number has a local maximum value and a local minimum value at heating temperatures of about 4 and 8°C, respectively, for a single water phase convection in a rectangular cavity, with a cooling temperature of 0°C.

As subcooling is maintained at one boundary, we are in the presence of a two phase ice–water problem, which has received much less attention. Results similar to that mentioned above may be expected while the existence of the ice–water interface, and the conduction in the ice, present additional complexities and constraints which would lead to some distinct phenomena.

The most recent literature dealing with the ice–water system was presented by Sasaki *et al.* [5]. They carried out a numerical study on the transient heat transfer process and found that the peculiar property of water at 4°C may result in a pair of counter-rotating vortices, and consequently the ice–water interface is curved with the top section thinner than the lower one and, therefore, the temperature field and heat transfer rates are qualitatively different from those of the Boussinesq fluid. They also found that the effect of density inversion could be neglected when the heating temperature is much higher than 4°C.

The purpose of the present paper is to study the two-phase convection in a water-saturated cavity which is, respectively, heated and cooled with temperatures higher and lower than the fusion temperature at the two vertical walls. Special attention is focused on the influence of the heating temperature on the interface shape, the heat transfer rate and the convection pattern. The technique of solving this problem consists of using the Landau-transformation to immobilize the ice–water interface, and the finite-difference control volume method to discretize the momentum and energy equations.

GOVERNING EQUATIONS

The physical system considered consists of a two-dimensional rectangular cavity filled with an ice–water porous medium. The horizontal boundaries of the

NOMENCLATURE

c_p	heat capacity [J kg^{-1}°C^{-1}]
g	gravitational acceleration [m s^{-2}]
H	height of the cavity [m]
k	conductivity [W m^{-1}°C^{-1}]
K	permeability [m^2]
L	length of the cavity [m]
Nu^h	average temperature gradient at the heated surface
Nu^c	multiple of the average temperature gradient at the cooled surface and $K_e^s/k_e^l \dot{T}_c/T_h$
Nu	Nusselt number at steady state, $Nu^h S$
q	constant in the water density expression, 1.894816
n	unit vector normal to the solid–liquid interface
P	pressure [N m^{-2}]
R	$k_e^s/k_e^l T_c/T_h$
Ra	Rayleigh number, $\lambda g(\Delta T^l)^q KH/(v\alpha_e^l)$
S	dimensionless interface position, S^*/H
T^l	dimensionless temperature in the liquid, $(T^{l*}-T_f^*)/\Delta T^l$
T_m	maximum density temperature, 4.029325 C
T^s	dimensionless temperature in the solid, $(T_f^*-T^{s*})/\Delta T^s$
T_h^*	superheating temperature [°C]
T_c^*	cooling temperature [°C]
T_f^*	fusion temperature [°C]
V	velocity in the liquid region [m s^{-1}]
x, y	Cartesian coordinates
XL	aspect ratio of the cavity, H/L.

Greek symbols

α_e^l	thermal diffusivity, $k_e^l/(\rho c)^l$ [m^2 s^{-1}]
ΔT^l	temperature scale in the liquid layer, $T_h^*-T_f^*$[°C]
ΔT^s	temperature scale in the solid layer, $T_f^*-T_c^*$[°C]
λ	constant in the water density expression, 9.297173×10^{-6} °C^{-q}
μ	viscosity [N s m^{-2}]
v	kinematic viscosity [m^2 s^{-1}]
ρ	density [kg m^{-3}]
ρ_m	maximum density of water at 4°C, 999.972 kg m^{-3}
ϕ	porosity
φ	dimensionless stream function, φ^*/α_e^l
Φ	either T, S or φ.

Superscripts

l	liquid
m	porous matrix
s	solid
*	dimensional variables.

Subscripts

e	effective property of the saturated porous medium
f	quantity at fusion point
m	maximum density point
max	maximum value
min	minimum value
0, 1	reference values.

cavity are adiabatic. The vertical walls are maintained at fixed temperatures T_c and T_h, respectively, below and above the fusion temperature T_f, i.e. 0°C, for the case of water considered here.

The mathematical description of the fluid flow is based on the Darcy model, assuming that:

(1) All physical properties are constant except for the density in the buoyancy force.
(2) The fluid is incompressible and its specific volume remains constant during the phase change process.
(3) Viscous dissipation is negligible.
(4) The flow is steady, laminar and two-dimensional.

The governing equations consist of:

the continuity equation

$$\nabla\cdot\mathbf{V}=0 \tag{1}$$

the momentum equation

$$\mathbf{V}=\frac{K}{\mu}(-\nabla P+\rho g) \tag{2}$$

the energy equation in the liquid region

$$\nabla\cdot(\mathbf{V}T^l-\alpha_e^l\nabla T^l)=0 \tag{3}$$

the energy equation in the solid region

$$\nabla^2 T^s=0 \tag{4}$$

and the energy balance at the interface

$$-k_e^l\nabla T^l\cdot\mathbf{n}+k_e^s\nabla T^s\cdot\mathbf{n}=0. \tag{5}$$

To describe the variation of density with temperature, the state equation of water proposed by Gebhart and Mollendorf [6] is used where, for water at atmospheric pressure

$$\rho=\rho_m(1-\lambda|T-T_m|^q). \tag{6}$$

By scaling length, velocity and temperatures to H, α_e^l/H and $\Delta T^l=T_h-T_f$ and $\Delta T^s=T_f-T_c$, the above equations can be expressed in the following dimensionless form:

$$\nabla^2\varphi+Ra\frac{\partial}{\partial x}|T-\beta|^q=0 \tag{7}$$

$$\nabla \cdot (\mathbf{V}T^{\mathrm{l}}) = \nabla^2 T^{\mathrm{l}} \quad (8)$$

$$\nabla^2 T^{\mathrm{s}} = 0 \quad (9)$$

$$0 = -\nabla_n T^{\mathrm{l}} + R\nabla_n T^{\mathrm{s}} \quad \text{(at the interface)} \quad (10)$$

where

$$Ra = \lambda g K(\Delta T^{\mathrm{l}})^q H/v\alpha_{\mathrm{e}}^{\mathrm{l}}$$

$$\beta = (T_{\mathrm{m}} - T_{\mathrm{f}})/(T_{\mathrm{h}} - T_{\mathrm{f}}) = 4/T_{\mathrm{h}}$$

$$R = k_{\mathrm{e}}^{\mathrm{s}}/k_{\mathrm{e}}^{\mathrm{l}} T_{\mathrm{c}}/T_{\mathrm{h}} \quad (11)$$

and the stream function φ is defined by

$$u = \frac{\partial \varphi}{\partial y}, \quad v = -\frac{\partial \varphi}{\partial x}. \quad (12)$$

To complete the mathematical formulation the above set of equations must satisfy the following boundary conditions:

$T = 1$ on the heated wall

$\frac{\partial T}{\partial n} = 0$ on the horizontal walls

$\varphi = 0$ on the interface and on the cavity walls

$T = 0$ on the interface

$T = -1$ on the cooled wall. (13)

It appears from the above mathematical formulation that the problem considered here is governed by four dimensionless parameters, namely the Rayleigh number Ra, the inversion parameter β, R, and the aspect ratio of the cavity XL.

In the present system, β is an indication of the location of the maximum density of water within the liquid region. In fact, in a pure convection state (i.e. if convection is neglected), β is just the relative position of the 4°C isotherm in the liquid layer. For example, $\beta = 0.5$ means that the maximum density line is at the middle of the liquid layer, $\beta = 1$ indicates that the maximum density line coincides with the vertical heated wall. The flow essentially depends on the value of this parameter. A more detailed discussion on the signification of this parameter can be found in the article of Nguyen *et al.* [7].

For a given porous matrix, fluid, cavity and subcooling temperature, the remaining parameters Ra, β, and R are interrelated to the superheating temperature T_{h}. The relation between two parameter groups (Ra_1, β_1, R_1) and (Ra_0, β_0, R_0) at heating temperatures $T_{\mathrm{h}1}$ and $T_{\mathrm{h}0}$, is

$$Ra_1 = Ra_0(T_{\mathrm{h}1}/T_{\mathrm{h}0})^q$$

$$\beta_1 = 4/T_{\mathrm{h}1}$$

$$R = R_0 T_{\mathrm{h}0}/T_{\mathrm{h}1} T_{\mathrm{c}1}/T_{\mathrm{c}0}. \quad (14)$$

Hereafter, in order to concentrate on the influence of the superheating temperature on the melting process, the various values of Ra, β and R will be expressed in terms of a reference set of values; $Ra_0 = 200$, $\beta_0 = 1$ and $R_0 = 3.667$, with $T_{\mathrm{h}0} = 4$°C. The conductivity ratio $k_{\mathrm{e}}^{\mathrm{s}}/k_{\mathrm{e}}^{\mathrm{l}}$ is chosen to be 3.667 which corresponds to cooling and heating temperatures of -4 and 4°C, respectively.

SOLUTION METHOD

In the presence of convection, the heat transfer rate along the solid–liquid interface is nonuniform. As a consequence, the shape of the interface is not a vertical line as in the case of conduction-dominated phase change, but becomes inclined and distorted proportionally to the local convective heat transfer rate along the interface. In order to deal with this difficulty in solving the governing equations, a curvilinear coordinate system was used to transform the irregular physical domain into a fixed rectangular one for the computational purpose [8].

A finite-difference method based on a control volume formulation was used to obtain the numerical solutions. The discretized equations were derived by using a power-law interpolation scheme. An iterative method was used to solve the discretized equations. At each iteration, the interface position S was determined from the energy balance at the interface. The stream function φ and temperatures T^{l} and T^{s} were then simultaneously solved from the momentum and energy equations. The position of the interface S was then recalculated using the φ and values of T, this procedure being repeated until convergent solutions were obtained. Usually, about 250 iterations were needed to obtain the steady solution. Steady solutions were assumed to have been attained when the difference between the two heat transfer rates on the heated and cooled sides differed by less than a predetermined tolerance, typically 3%. Details of the numerical scheme can be found in Zhang *et al.* [8].

RESULTS AND DISCUSSION

Numerical results have been obtained for heating temperatures ranging from 2 to 12°C. Effects of subcooling and aspect ratio were considered by choosing values of $T_{\mathrm{c}} = -2$, -4°C and $XL = 1$, 2.5. Results were also obtained for two groups of reference values of $Ra_0 = 40$, $\beta_0 = 1$ at $T_{\mathrm{h}0} = 4$°C and $Ra_1 = 80$, $\beta_1 = 1$ (corresponding to $T_{\mathrm{h}1} = 4$°C) in order to investigate separately the effect of Rayleigh number.

Temperature and flow fields

The isotherms and streamlines for steady states of an ice–water system subjected to a fixed subcooling temperature $T_{\mathrm{c}} = -2$°C and a heating temperature T_{h} varying from 2 to 12°C are illustrated in Figs. 1(a)–(i), for reference values Ra_0, R_0, β_0, $T_{\mathrm{h}0}$ and XL_0.

Figure 1(a) shows the flow pattern (left) and the isotherms (right) for $T_{\mathrm{h}} = 2$°C (in all these and the following figures, the left vertical wall is cooled and the right vertical wall is heated). This situation is dominated by conduction in both the solid and liquid phases, as indicated by the almost vertical isotherms.

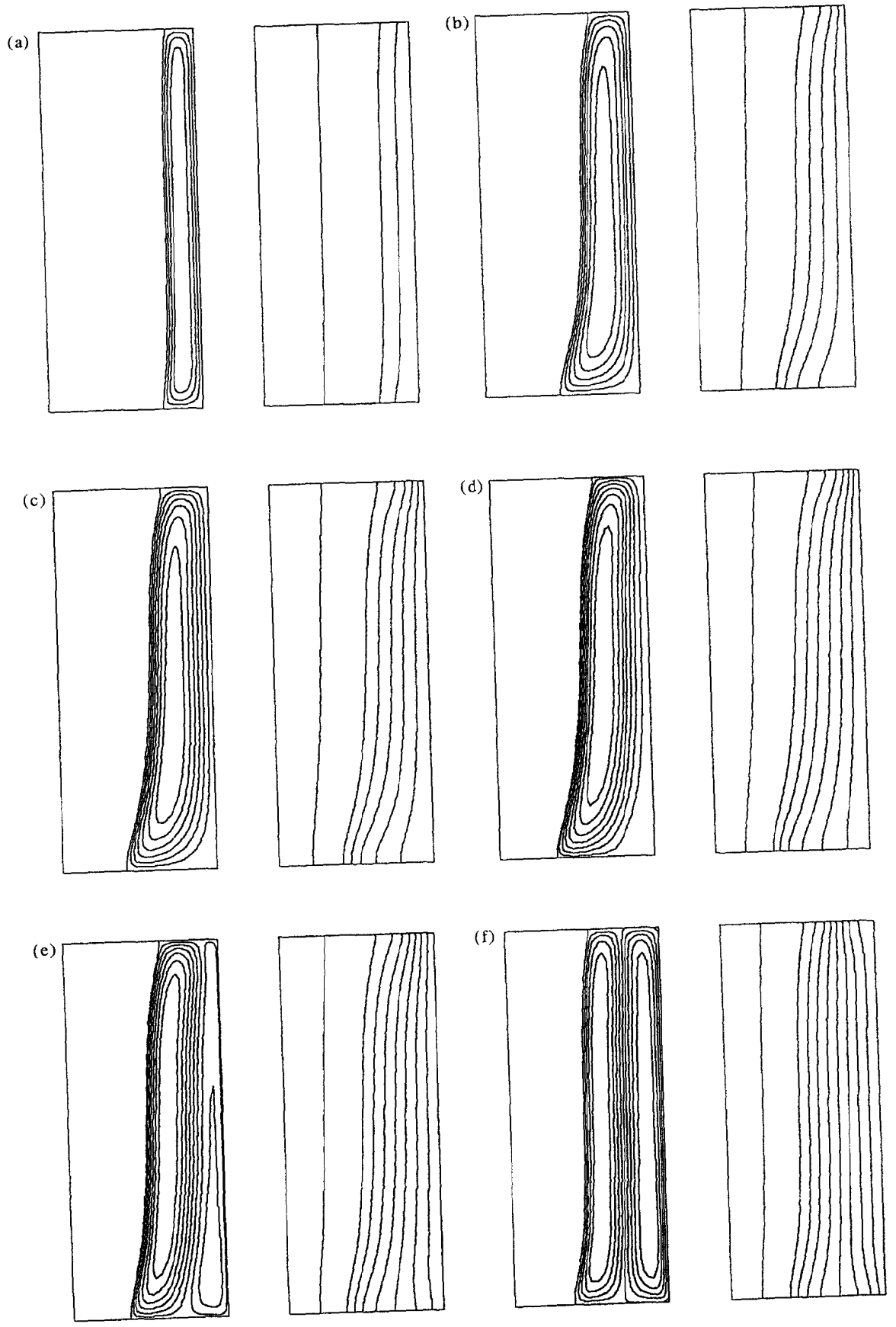

FIG. 1.

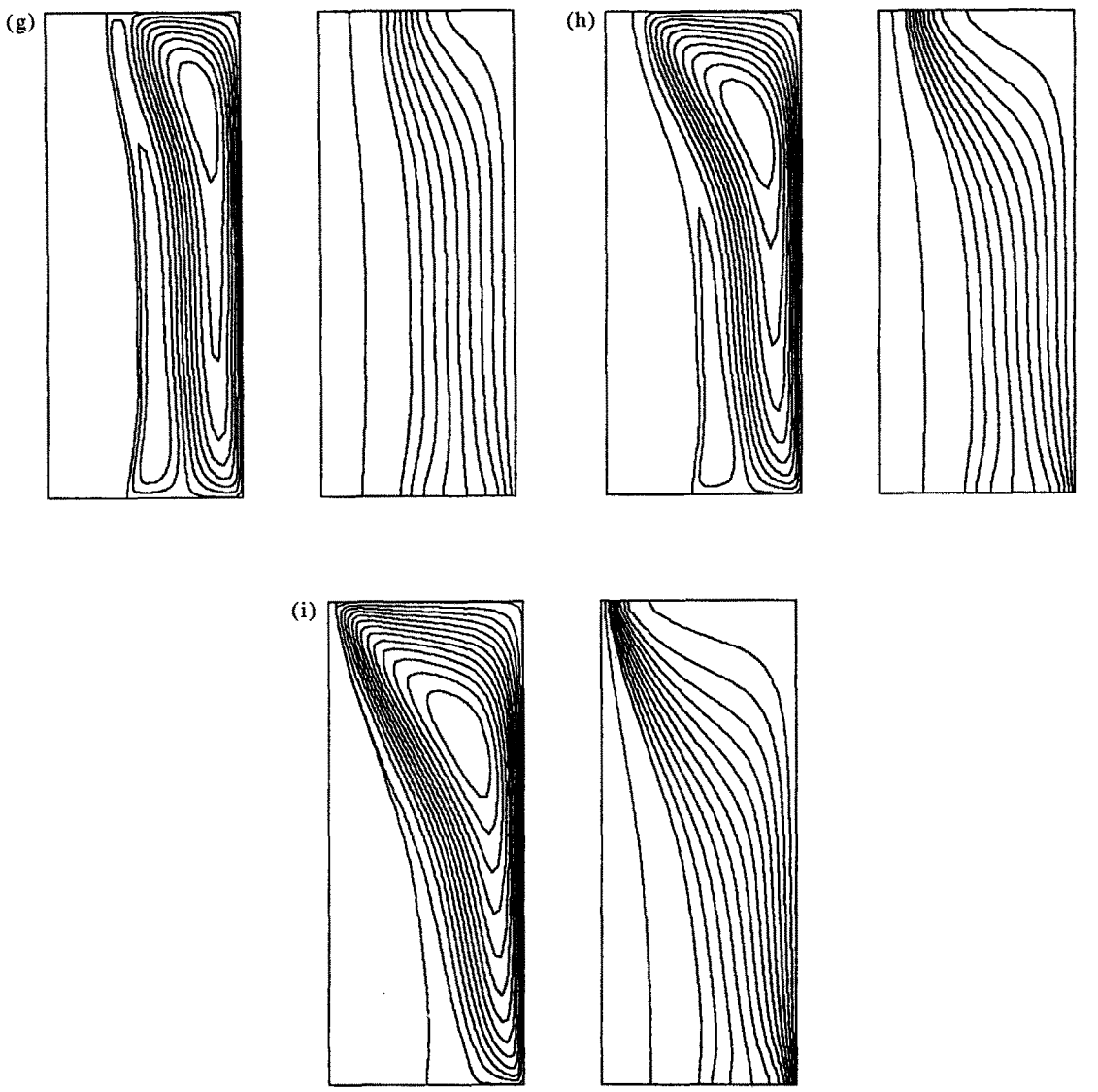

FIG. 1. Streamlines and isotherms (isotherm spacing: 1°C). $Ra_0 = 40$, $T_{c0} = -2$°C, $T_{h0} = 4$°C, $XL = 2.5$. (a) $T_h = 2$°C, (b) $T_h = 4$°C, (c) $T_h = 5$°C, (d) $T_h = 6$°C, (e) $T_h = 7$°C, (f) $T_h = 8$°C, (g) $T_h = 9$°C, (h) $T_h = 10$°C, (i) $T_h = 12$°C.

The convective flow induced by the horizontal temperature gradient is very weak and has a negligible effect on the temperature distribution within the system. It is, however, worth noting that although the fluid adjacent to the ice–water interface is cooler, it is lighter than the fluid adjacent to the heated wall, due to the peculiar behavior of water in the 0–4°C temperature range. As a consequence, one observes here a clockwise circulation with the fluid descending along the heated wall and rising along the interface, contrary to the case of a normal fluid whose density is a monotonous decreasing function of temperature.

The case $T_h = 4$°C is shown in Fig. 1(b) where the effect of convection becomes visible in the end regions: the melt is thinner and the isotherms are more closely spaced in the upper part than in the lower part of the cavity. This effect is due to the fact that heat is convected downward from the side wall to the lower part of the cavity, in opposition to the case of a normal fluid which rises along the heated wall and impinges on the upper part of the interface to create a wider melt in that region. One could also note from this figure that the streamlines are more closely spaced, i.e. the fluid moves faster along the interface than along the heated wall. This result is characteristic of the nonlinear relationship between density and temperature of water that makes the density gradient vanish across the 4°C isotherm and thereby considerably weakens the buoyancy flow.

Figure 1(c) shows the case of a heating temperature $T_h = 5$°C. The results are quite similar to the previous case, except for the fact that the melt volume is slightly greater. This situation is, however, significant in that one observes only a clockwise circulation, although

the 4°C isotherm is now located within the flow domain and one might expect the possible development of flow reversal. In fact, the occurrence of the latter is still retarded by the shear force of the main clockwise vortex which entrains the light fluid layer between the 4 and 5°C isotherms into its downward motion.

The streamlines and isotherms corresponding to a heating temperature $T_h = 6$°C are presented in Fig. 1(d). Here one observes the appearance of a secondary counterclockwise vortex at the lower right corner of the cavity. For the reason just mentioned above, this reverse flow does not occupy the whole 4–6 C layer, but just a small region where viscous shearing can no longer dominate the upward buoyancy. In fact, as the heating temperature is further increased, the reverse flow becomes stronger and stronger as can be seen from Figs. 1(e) and (f) for $T_h = 7$ and 8°C, respectively. At $T_h = 8$°C, one notes that the maximum density (the 4°C isotherm) is located approximately in the middle of the melt region while the fluid along the heated wall has the same density as that along the interface, resulting in two counter-rotating vortices of approximately the same size and strength. It can be noted in passing that in a rectangular cavity with wide walls maintained respectively at 0 and 8°C, the flow consists of two mirror image vortices across the 4°C isotherm (located at the mid-plane of the cavity). In the present ice–water system, the shape of the interface is controlled by the local heat transfer rate so that the melt region is slightly wider in the lower part than in the upper part, hence destroying the symmetry between the two vortices.

Moreover, from the isotherm pattern in Fig. 1(f) it can readily be seen that, except at the upper and lower ends of the cavity, the isotherms are almost vertical and equally spaced. Convective heat transfer is thus greatly reduced compared to the case of heating at a lower $T_h = 4$ C where, in the absence of density inversion, only a unicellular flow can develop.

Results for heating temperatures $T_h = 9$, 10 and 12 C are presented in Figs. 1(g)–(i). As T_h increased beyond 8°C, the counterclockwise vortex adjacent to the heated wall becomes stronger and stronger to completely dominate the flow domain when $T_h = 12$°C. As a consequence, the melt at the top of the cavity becomes larger than at the bottom, as in the case of a normal fluid whose density decreases with increasing temperature.

Heat transfer rate

Closely related to the temperature and flow fields discussed above is the heat transfer rate which can be expressed in terms of the local Nusselt numbers as well as the overall Nusselt number.

It should be noted that for steady states, the overall Nusselt numbers at both side walls must be equal. In fact, this is the condition imposed on the convergence of the numerical solutions.

Referring to the isotherms in Fig. 1, it can be readily seen that for $T_h < 7$°C the local heat transfer rate along the heated wall increases upward, i.e. the Nusselt number is maximum at the top and minimum at the bottom of the side wall. The inverse is true along the interface. This is due to the fact that for $T_h < 7$°C, the dominant flow is clockwise, with the hot fluid moving down the side wall to impinge on the lower end of the interface. Along the cooled wall, the Nusselt number decreases upward, due to the fact that the solid phase is narrower in the lower part of the cavity.

At $T_h = 8$°C, the convection becomes weaker and the heat transfer rate is almost uniform along the side walls and the interface, as can be deduced from the almost parallel isotherms in Fig. 1(f).

For $T_h > 8$°C, the above tendency is reversed, i.e. the Nusselt number increases downward along the heated side wall and upward along the interface, as a consequence of the counterclockwise flow.

The effect of heating temperature on the Nusselt number is illustrated in Fig. 2(a) which shows Nu vs T_h for reference values $Ra_0 = 40$, $XL_0 = 2.5$, and $T_{c0} = -2$°C at $T_{h0} = 4$ C.

In a normal fluid, increasing the heating temperature amounts to proportionally increasing the Rayleigh number, thereby increasing the heat transfer rate. In the present case however, Fig. 2(a) shows that Nu first increases with T_h to attain a maximum value at $T_h \approx 5$°C and decreased afterward to a minimum value at $T_h = 8$°C before increasing again with T_h. This behavior is the result of the interplay between the two opposing effects: on the one hand, an increase of heating temperature corresponds to an increase of Rayleigh number and therefore to a higher heat transfer rate, but on the other hand it also induces an increasing flow reversal in the range $4 \leqslant T_h \leqslant 8$°C, which has a damping effect on the convection heat transfer.

The occurrence of a maximum Nusselt number at $T_h \approx 5$°C is due to the fact that when T_h is increased from 0 to 4°C, the Rayleigh number is increased accordingly while no inversion phenomenon is possible. When T_h is increased from 4 to 5°C, the Rayleigh number continues to increase and, as described in the previous section, viscous entrainment is strong enough to suppress the onset of flow reversal. The flow at $T_h = 5$°C is therefore still unicellular and heat is directly transferred from the heated wall to the ice–water interface. The Nusselt number then reaches a maximum value at the end of the unicellular flow regime. This result, indeed, confirms the conjecture that an optimum heating in the presence of density inversion would be the one for which the fluid motion consists of a single cell [9].

For the geometry considered here, the inversion effect appears to be maximum when $T_h = 8$°C, thus reducing the Nusselt number to a minimum value at that temperature.

It should be noted that while the occurrence of a maximum heat transfer rate at $T_h = 5$°C has not been

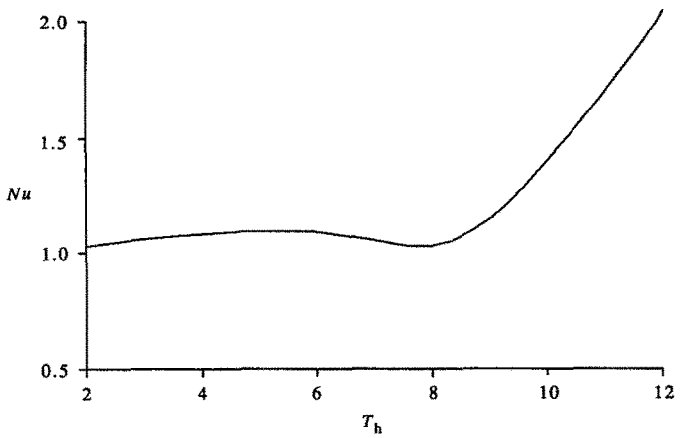

FIG. 2(a). Nusselt numbers vs heating temperature. $Ra_0 = 40$, $T_{c0} = -2°C$, $T_{h0} = 4°C$, $XL = 2.5$.

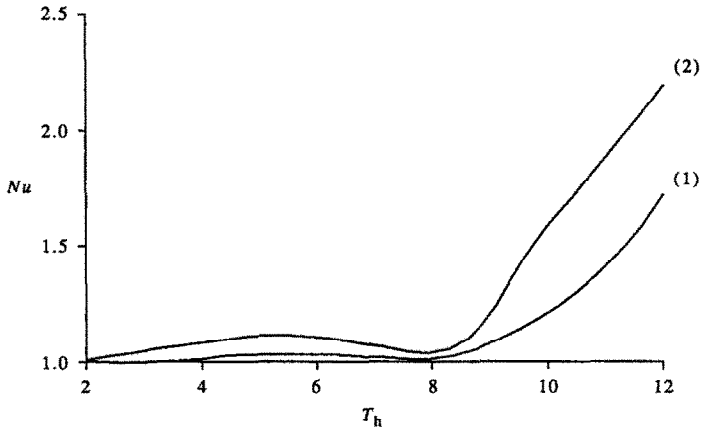

FIG. 2(b). Nusselt numbers vs heating temperature. $T_{c0} = -4°C$, $T_{h0} = 4°C$, $XL = 2.5$. (1) $Ra_0 = 40$; (2) $Ra_0 = 80$.

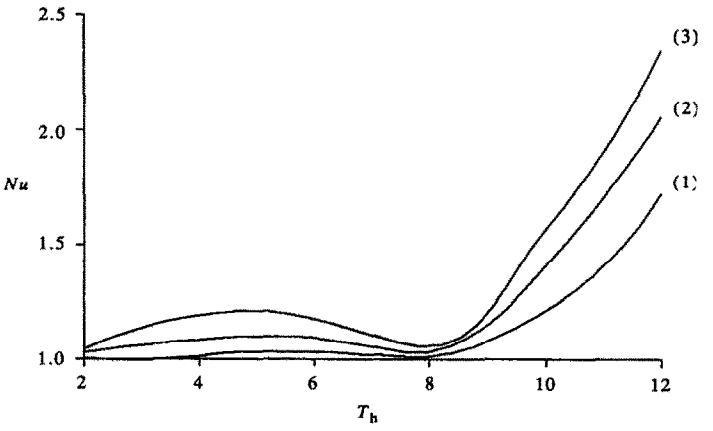

FIG. 2(c). Nusselt numbers vs heating temperature. $Ra_0 = 40$, $T_{h0} = 4°C$, $XL = 2.5$. (1) $T_{c0} = -4°C$; (2) $T_{c0} = -2°C$; (3) $T_{c0} = -1°C$.

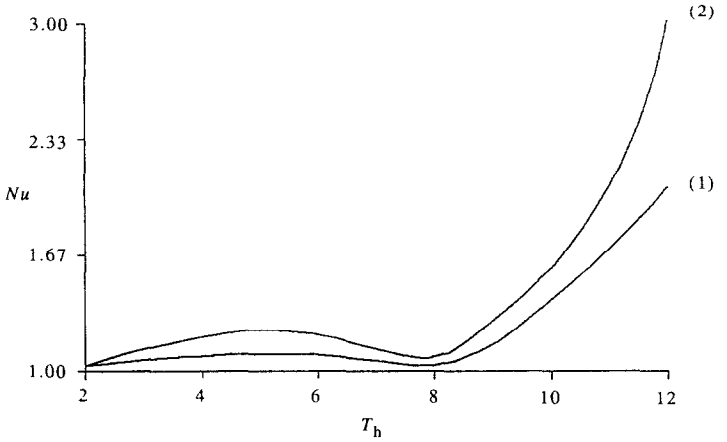

FIG. 2(d). Nusselt numbers vs heating temperature. $Ra_0 = 40$, $T_{c0} = -2$ C, $T_{h0} = 4$ C. (1) $XL = 2.5$; (2) $XL = 1.0$.

reported in previous studies, many authors have observed numerically and experimentally a minimum heat transfer rate in various ice–water systems.

Bendell and Gebhart [10] have experimentally studied the problem of natural convection over a vertical ice slab and found that when the ambient temperature $T = 5.6$°C the flow is downward while it is upward for $T = 5.5$°C. In the experimental range $2.2 < T < 25$°C, a minimum Nusselt number was obtained at $T = 5.6$°C.

Rieger and Beer [11], in a numerical and experimental study on the melting of ice inside a horizontal cylinder, found a minimum Nusselt number at a wall heating temperature $T \approx 8$°C.

In a numerical simulation of the melting of ice around a heated horizontal cylinder, Ho and Chen [12] obtained a minimum heat transfer rate during the early stage of the melting process (i.e. for dimensionless time $\tau < 0.2$) when the wall heating temperature $T = 8$°C, and at later times ($\tau > 0.2$) when the heating temperature $T = 9$°C.

The above results are obtained at the reference values $Ra_0 = 40$, $\beta_0 = 1$, $T_{h0} = 4$°C, $XL_0 = 2.5$ and $T_{c0} = -2$°C. In order to see the dependence on other parameters of the system, Figs. 2(b) and (c) are presented. Figure 2(b) shows two curves of Nu vs T_h for two different groups of reference values, $Ra_0 = 40$, $\beta_0 = 1$, $T_{c0} = -4$°C, $T_{h0} = 4$°C and $Ra_1 = 80$, $\beta_1 = 1$, $T_{c1} = -4$°C, $T_{h1} = 4$°C. At a given value of T_h, β is the same in the two cases, but the corresponding Rayleigh number is twice as big. Doubling the Rayleigh number at various values of T_h then results in a monotonous increase of the Nusselt number as can be expected.

The effect of subcooling on the heat transfer rate is illustrated in Fig. 2(c) which shows Nu vs T_h for three different values, $T_c = -1$, -2 and -4°C at $Ra_0 = 40$, $\beta_0 = 1$, $T_{h0} = 4$°C. It should be noted in interpreting this figure that when the subcooling temperature is increased from -4 to -1°C, with other parameters being fixed, the melt volume also increases, resulting in a larger flow domain and hence a stronger convection flow. The increase of Nusselt number with the cooling temperature, as shown in Fig. 2(c), is therefore similar to that observed in the previous figure with an increasing Rayleigh number.

Figure 2(d) shows the curve of Nu vs T_h for two aspect ratios $XL = 1$ and 2.5, at reference values $Ra_0 = 40$, $\beta_0 = 1$, $T_{c0} = -2$°C, $T_{h0} = 4$°C. It should be noted that as XL is increased, the width of the cavity is decreased. The melt volume is therefore reduced accordingly. A larger aspect ratio is thus qualitatively similar to a lower subcooling. In fact, by comparing Figs. 2(b)–(d), it appears that the Rayleigh number, subcooling temperature and aspect ratio have comparably strong effects on the heat transfer rate in the ranges of parameters considered in this study.

Interface shape

At steady state, the shape and position of the solid–liquid interface provide information concerning the melt fraction as well as the heat transfer rate between the solid and liquid phases: a straight (vertical) interface indicates that the heat transfer rate is uniform along the interface, and along the side walls. This situation can occur if the system is governed by conduction alone, i.e. if natural convection effects are negligible. Generally, the interface is curved due to the nonuniform heat transfer along the interface and side walls, due to the effects of natural convection in the liquid region. In fact, it has been well recognized that the melt region of a normal phase change material (PCM) is always thicker at the top of the cavity, and the interface advances towards the cooled wall as the heating temperature or the subcooling temperature is increased. This, however, is not true in the case of the ice–water system considered here, as can be seen from

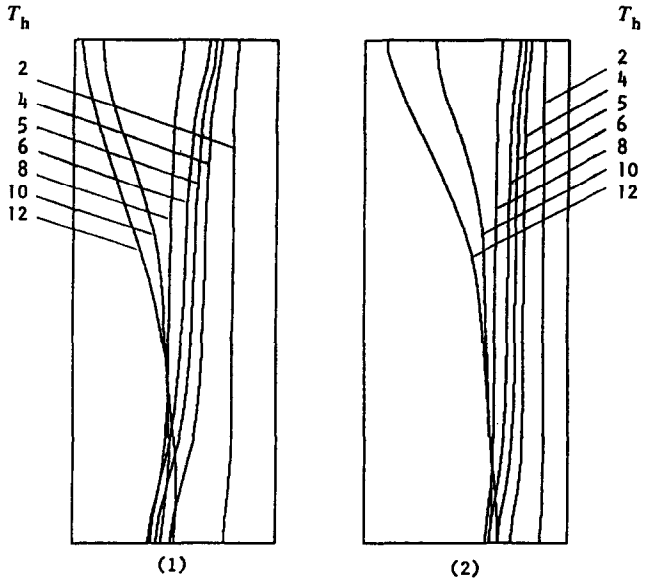

FIG. 3. Interface shapes at different heating temperatures. $Ra_0 = 40$, $T_{h0} = 4°C$, $XL = 2.5$. (1) $T_c = -2°C$; (2) $T_c = -4°C$.

Figs. 3(1) and (2) which show the interface positions corresponding to a heating temperature varying from 2 to 12°C and a subcooling temperature of −2 and −4°C, respectively, at reference values $Ra_0 = 40$, $T_{h0} = 4°C$, $T_{c0} = -2°C$. From these figures, it appears that the melt volume increases, when the heating temperature increases from 2 to 12°C. In the 0–8°C heating range, the lower part of the melt is wider than the upper one, in opposition to the case of a normal PCM. As the heating temperature is increased beyond 8°C, the melt thickness at the lower part of the cavity decreases while that at the upper part increases. The melt then becomes wider in the top of the cavity as in the case of a normal PCM.

Values of heat transfer rates and interface positions corresponding to various heating temperatures are presented in Table 1 for the cases with $T_{c0} = -4°C$, $T_{h0} = 4°C$ and $Ra_0 = 40$.

Table 1. Nusselt number and interface position for: $Ra_0 = 40$, $T_{h0} = 4°C$, $T_c = -4°C$

T_h (°C)	Nu	S_{ave}	S_{max}	S_{min}
2	1.002	0.1202	0.1309	0.1112
4	1.010	0.2175	0.2754	0.1772
4.5	1.025	0.2391	0.3092	0.1906
5	1.030	0.2595	0.3385	0.2037
6	1.029	0.2958	0.3802	0.2313
7	1.019	0.3267	0.3989	0.2651
8	1.009	0.3547	0.3999	0.3187
10	1.207	0.4419	0.6483	0.3651
12	1.720	0.5156	0.8908	0.3403

CONCLUSION

A numerical study has been made of the steady state convection flow and heat transfer in an ice–water saturated porous medium. The results can be summarized as follows.

(1) The Rayleigh number, subcooling temperature and aspect ratio have a strong and similar influence on the heat transfer rate as well as on the position and the shape of the solid–liquid interface.

(2) The density inversion of water plays a determinant role in the flow pattern and the ice–water interface position such that:

(i) For $T_h < 5°C$, the flow is unicellular with the fluid descending along the heated wall, creating a thicker melt layer in the lower part of the cavity.

(ii) For $T_h > 12°C$, the flow is unicellular with the fluid moving up along the heated wall, creating a thicker melt layer in the upper part of the cavity.

(iii) For $5 \leqslant T_h < 12°C$, the flow consists of two counter-rotating vortices of unequal size, such that for $5 \leqslant T_h \leqslant 8°C$, the melt is thicker in the lower part of the cavity, while the inverse is true for $8 < T_h < 12°C$.

(3) The heat transfer rate is strongly affected by the density inversion in such a way that the average Nusselt number first increases with the heating temperature until $T_h = 5°C$, but decreases afterwards to reach a minimum value at $T_h = 8°C$ before increasing again with the heating temperature.

Acknowledgement—This study was supported by the Natural Sciences and Engineering Research Council of Canada under grant Nos. OGP0000626 and OGP121621.

REFERENCES

1. P. Jany and A. Bejan, The scales of melting in the presence of natural convection in a rectangular cavity filled with porous medium, *J. Heat Transfer* **110,** 526–529 (1988).
2. A. Bejan, Theory of melting with natural convection in an enclosed porous medium, *J. Heat Transfer* **111,** 407–415 (1989).
3. H. Inaba and T. Fukuda, An experimental study of natural convection in an inclined rectangular cavity filled with water at its density extremum, *J. Heat Transfer* **106,** 109–115 (1984).
4. C. Tien, Thermal instability of a horizontal layer of water near 4°C, *A.I.Ch.E. Jl* **14,** 652–655 (1968).
5. A. Sasaki, S. Aiba and S. Fukusako, Numerical study on freezing heat transfer in water-saturated porous media, *Numer. Heat Transfer, Part A* **18,** 17–32 (1990).
6. B. Gebhart and J. Mollendorf, A new density relation for pure and saline water, *Deep-Sea Res.* **124,** 831–848 (1977).
7. T. H. Nguyen, P. Vasseur and L. Robillard, Natural convection between horizontal concentric cylinders with density inversion of water for low Rayleigh numbers, *Int. J. Heat Mass Transfer* **25,** 1559–1568 (1982).
8. X. Zhang, T. H. Nguyen and R. Kahawita, Melting of ice in a porous medium heated from below, *Int. J. Heat Mass Transfer* **34,** 389–405 (1991).
9. G. Veronis, Penetrative convection, *Astrophys. J.* **137,** 641–663 (1963).
10. M. Bendell and B. Gebhart, Heat transfer and ice-melting in ambient water near its density extremum, *Int. J. Heat Mass Transfer* **19,** 1081–1087 (1976).
11. H. Rieger and H. Beer, The melting process of ice inside a horizontal cylinder : effects of density anomaly, *J. Heat Transfer* **108,** 166–173 (1986).
12. C. J. Ho and S. Chen, Numerical simulation of melting of ice around a horizontal cylinder, *Int. J. Heat Mass Transfer* **29,** 1369–1369 (1986).